Research Article
Vol. 27, No. 9 | 29 Apr 2019 | OPTICS EXPRESS 13194
Optics EXPRESS

High-resolution phased array radar imaging by photonics-based broadband digital beamforming

Bindong Gao,[1] Fangzheng Zhang, [1,2] Ermao Zhao,[1] Daocheng Zhang[1] and Shilong Pan[1,3]

[1]*Key Laboratory of Radar Imaging and Microwave Photonics, Ministry of Education, Nanjing University of Aeronautics and Astronautics, Nanjing 210016, China*
[2]*zhangfangzheng@nuaa.edu.cn*
[3] *pans@nuaa.edu.cn*

Abstract: A photonics-based broadband phased array radar is demonstrated to realize high-resolution imaging based on digital beamforming. This photonics-based phased array radar can achieve a high range resolution enabled by a large operation bandwidth, and can realize squint-free beam steering by digital true time delay (TTD) compensation. In addition, the photonic dechirp processing applied in the receiver can alleviate the hardware requirements for data sampling and storage, and hence remarkably enhance the real-time signal processing capability. In a proof-of-concept experiment, target imaging by a photonics-based 1 × 4 phased array radar that has a bandwidth of 4 GHz (22-26 GHz) is demonstrated, of which the range and azimuth resolution is measured to be 3.85 cm and 2.68°, respectively. The proposed scheme provides good solution to overcoming the bandwidth limitation and implementing high-resolution imaging in a phased array radar.

1. Introduction

Radar imaging plays an important role in many applications such as security check, automatic driving, ocean monitoring and so on [1,2]. As a promising technology, target imaging by beamforming with a phased array radar can achieve a high azimuth resolution without mechanically moving the radar platform. While, current phased array radars usually work in a narrow band, which severely limits the range resolution of the radar. The main factors limiting the operation bandwidth of a phased array radar include: i) the bandwidth of electrical devices and subsystems is limited, e.g., the bandwidth of a DDS is constrained to a few GHz [3]; ii) the main-beam squint problem makes it difficult for a phased array radar to operate at a broad frequency band [4].

To overcome the bandwidth limitation of electronic systems, microwave photonic technologies have been proposed and extensively investigated [5,6]. Until now, many photonics-based broadband radars have been demonstrated with the potential to improve the range resolution of a traditional radar by an order of magnitude [7–10]. Based on these systems, high resolution inverse synthetic aperture (ISAR) imaging is demonstrated [11–13]. In addition to monostatic radars, photonics-based broadband distributed and multiple-input-multiple-output (MIMO) radars have also been successfully demonstrated [14,15]. Provided the radar bandwidth can be greatly enhanced by microwave photonic technologies, the main-beam squint problem due to the aperture effect and the aperture traverse delay still constrains the operation bandwidth of a phased array radar. To achieve squint-free beam steering in a broadband phase array radar, true time delay (TTD) technique is required. Thanks to the low-loss transmission property, photonics-based TTD schemes applying optical fiber delay line have been proposed [16–20], of which the operation principle has been proved feasible. However, these schemes suffer from high complexity, large volume and poor stability.

#358901 https://doi.org/10.1364/OE.27.013194
Journal © 2019 Received 28 Jan 2019; revised 4 Apr 2019; accepted 5 Apr 2019; published 25 Apr 2019

Besides, the TTD resolution is usually limited, e.g., a resolution of ~69 ps was achieved in [17]. These factors severely hinder the practical applications of photonic TTD techniques.

In this paper, we propose a photonics-based broadband phased array radar for high resolution imaging based on digital beamforming. The radar transmits a broadband linearly frequency modulated (LFM) signal generated by photonic frequency multiplication. In each receive channel, photonics-based dechirping is implemented to obtain the 1D range profile. After digitally compensating for the TTD, digital beamforming is performed to construct a 2D image. The proposed photonics-based phased array radar achieves a high range resolution thanks to the large operation bandwidth. Besides, it solves the main-beam squint problem by simple digital TTD compensation, avoiding the use of complicated physical TTD network and also strengthening the processing flexibility. Furthermore, the broadband photonic dechirp processing alleviates the hardware requirements for digital sampling and storage in each receiver, and enhances the signal processing capability for real-time and high-resolution imaging.

2. Principle of the photonics-based phased array radar

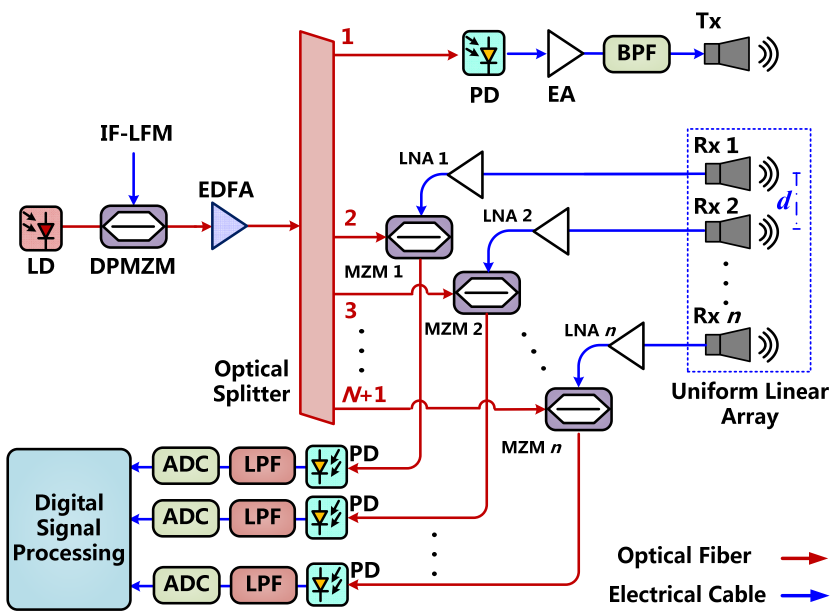

Fig. 1. Setup of the photonics-based phased array radar. LD: laser diode; OC: optical coupler; DPMZM: dual-parallel Mach-Zehnder modulator; EDFA: erbium-doped fiber amplifier; PD: photodetector; EA: electrical amplifier; PA: power amplifier; LNA: low noise amplifier; MZM: Mach-Zehnder modulator; LPF: electrical low-pass filter; ADC: analog-to-digital converter.

Figure 1 shows the setup of the photonics-based phased array radar with 1 transmitter and N receivers. A continuous-wave (CW) light emitted by a laser diode (LD) is sent to a dual-parallel Mach-Zehnder modulator (DPMZM), which is driven by an intermediate frequency (IF)-band LFM signal generated by a low-speed electrical signal generator. By properly setting the bias voltages of the DPMZM, the output optical signal only includes the ± 2nd order modulation sidebands [21]. After power amplification by an erbium-doped fiber amplifier (EDFA), this optical signal is split into $N + 1$ branches by an optical splitter. The signal in the first branch is sent to a photodetector (PD) to implement optical-to-electrical conversion, and an LFM signal is generated, of which the frequency and bandwidth are quadrupled compared with the IF-band LFM signal. The optical signal in the other N branches is used as the reference signals of the radar receivers. The generated LFM signal is amplified by an electrical amplifier (EA) and passed through a band-pass filter (BPF) to suppress the out-of-band noises and spurs, before emitted to the detection area through a transmit antenna. The radar echoes reflected from the target are collected by the receive antennas of the N receivers, which compose a uniform linear array (ULA) with an element spacing of d. The signal collected by each antenna is first amplified by a low noise amplifier (LNA) and then fed to an MZM to modulate an optical reference signal. The output signal from each MZM is sent to a PD to perform photonic frequency mixing. This way, photonics-based de-chirping of the received radar echo is implemented [8]. The de-chirped signal is filtered out by a low-pass filter (LPF) and sampled by an analog-to-digital converter (ADC). The obtained N-channel digital signals are sent to a digital signal processing (DSP) unit.

In the DSP unit, to deal with the aperture effect, which causes the broadband beam squinting in traditional phased array radars, digital TTD compensation is implemented. To do this, a point reference target is used to obtain the time delay difference between the four receive channels. Firstly, the 1D range profile corresponding to each receiver is calculated by performing Fast Fourier Transformation (FFT), which can be expressed as [8]:

$$R_i(r) = \left\{F\left[S_i(t)\right]\right\}_{f=2kr/c} \tag{1}$$

where $F(\cdot)$ denotes the FFT operation, $S_i(t)$ is the sampled de-chirped signal of the i-th receiver ($i = 1, 2, \ldots, N$), k is the chirp rate of the transmitted LFM signal, and c is the wave propagation speed. In obtaining Eq. (1), the frequency of the spectral peak corresponding to the point target in $F[S_i(t)]$ are also obtained. By comparing the frequency of the spectral peak in each receiver with that of the referenced receiver of the ULA, the true time delay between a specific receiver and the referenced receiver can be obtained by:

$$\tau_i = \Delta f_i / k \tag{2}$$

where Δf_i is the frequency difference between the spectral peak of $F[S_i(t)]$ in the i-th receive channel and spectral peak in the referenced receive channel of the ULA. Once the true time delay is known, digital TTD compensation can be implemented in frequency domain by:

$$R_i^{'}(r) = \left\{F\left[S_i(t)\right]\cdot e^{j2\pi f \tau_i}\right\}_{f=2kr/c} \tag{3}$$

where j is the imaginary unit. After digital TTD compensation, a 1D range-profile matrix can be obtained as:

$$\mathrm{R}(r) = [R_1^{'}(r) \quad R_2^{'}(r) \quad \ldots \quad R_N^{'}(r)] \tag{4}$$

The steering vector matrix is given as

$$\Phi(\theta) = [1 \quad e^{2\pi f_c d\sin\theta/c} \quad \ldots \quad e^{2\pi f_c (N-1) d\sin\theta/c}] \tag{5}$$

where f_c, and θ denotes the center frequency of the transmitted signal and the scanning angle in azimuth, respectively. Finally, radar imaging realized by digital beamforming can be implemented by

$$\mathrm{I}(r,\theta) = \mathrm{R}(r)\cdot\Phi^T(\theta) \tag{6}$$

where $(\cdot)^T$ denotes the transposition operation. In practical applications, by sweeping the azimuth angle at different range-resolution units based on Eq. (6), a 2D image can be derived. The range-resolution is determined by the radar bandwidth, i.e.,

$$L_{RES} = \frac{c}{2B} \tag{7}$$

where B is the bandwidth of the transmitted LFM signal. The azimuth resolution is given as [22]

$$\theta_{RES} \approx \frac{1}{\cos\theta_s} \frac{0.886c}{Nd \cdot f_c} \tag{8}$$

where θ_s denotes the desired beam angle with respect to the normal of the antenna array.

In this photonics-based phased array radar, broadband LFM signal generation and processing can be implemented because of the use of microwave photonic techniques, which ensures a high range resolution. In realizing squint-free beam steering, simple and flexible digital TTD compensation is applied to avoid the complicated physical TTD network required in analog beam steering. The photonic dechirping is a broadband zero-IF frequency mixing process, of which the output dechirped signal locates in the low frequency region. This property not only alleviates the hardware requirements for data sampling and storage in each receiver, but also enhances the real-time signal processing capability for the digital TTD compensation and digital beamforming.

3. Experimental demonstration

To verify the feasibility of the proposed photonics-based phased array radar, an experiment is carried out by establishing a 1 × 4 phased array radar. In the experiment, the CW light source is generated by an LD (TeraXion NLL04) at 1550.51 nm with a power of 17 dBm. The DPMZM (Fujitsu FTM7962EP) has a 3-dB bandwidth of 28 GHz. It is driven by a continuous-wave IF-LFM signal generated by an arbitrary waveform generator (Tektronix, AWG70001A). The bandwidth and repetition rate of the IF-LFM signal is 1 GHz (5.5-6.5 GHz) and 100 kHz, respectively. After biasing the DPMZM at the quadrupling mode, the output signal is monitored by an optical spectrum analyzer (Yokogawa AQ6370C, resolution: 0.02 nm). Figure 2(a) shows the measured spectrum, where two frequency sweeping ± 2nd-order optical sidebands are generated with the optical carrier suppressed by 20 dB. This optical signal is amplified by an erbium doped fiber amplifier (EDFA, Amonics Ltd.) with a gain of ~20 dB, and an OBPF (Yenista, XTM-50) is followed to suppress the undesired sidebands and the amplification of spontaneous emission (ASE) noise. Then, the obtained optical signal is split into two branches by a 50:50 optical coupler (OC). The signal from one branch sent to a broadband PD (u2t XPDV2120RA, bandwidth: 40 GHz) to perform optical-to-electrical conversion. The generated LFM signal has a bandwidth of 4 GHz, covering a frequency range of 22 GHz to 26 GHz. This LFM signal is first amplified by a broadband EA (CONNPHY, CMP-0.1G40G-3020-K), and then filtered by a band-pass filter (operation bandwidth: 22-26 GHz). The electrical spectrum of the generated LFM signal is measured by an electrical spectrum analyzer (ESA, R&S FSV40), as shown in Fig. 2(b), in which the temporal waveform of the LFM signal measured by a real-time oscilloscope (Keysight DSO-X 92504A, sampling rate: 80 GHz) is included in the inset. As shown in Fig. 2(b), the LFM signal covering 22-26 GHz is successfully generated and the signal-to-noise ratio (SNR) reaches 47 dB.

Optics EXPRESS

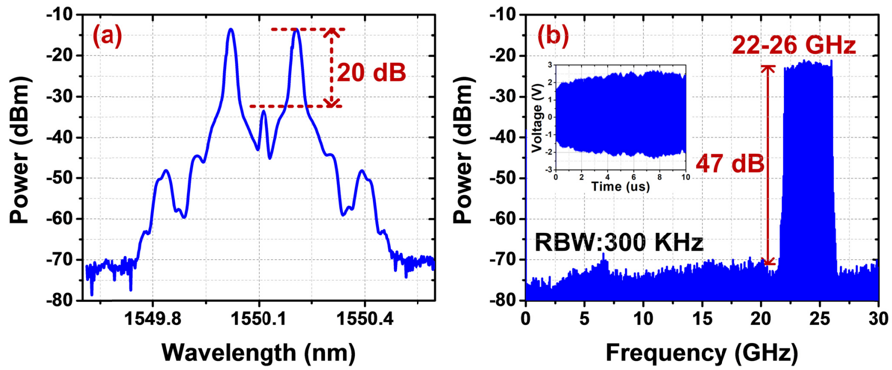

Fig. 2. (a) Optical spectra of the frequency quadrupling modulated signal; (b) spectrum of the generated LFM signal in 22-26 GHz (RBW = 300 kHz, inset: waveform of the LFM signal).

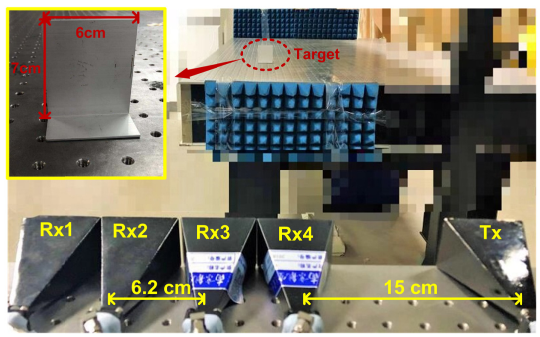

Fig. 3. Photograph of the antennas and target in the experiment.

The generated LFM signal is emitted to the detection area through a horn antenna, of which the operation bandwidth and gain is 18-26.5 GHz and 20 dBi, respectively. The radar echoes are collected by four receive antennas having the same parameters with that of the transmit antenna. The ULA composed by the four receive antennas has an element spacing of 6.2 cm, and the spacing between the transmit antenna and first receive antenna is 15 cm, as shown in Fig. 3. In this case, the far-filed condition is satisfied when the target is separated from the radar by over 2 meters. In each receiver, the echo signal is amplified by a LNA (CONNPHY) and used to drive an MZM (Fujitsu FTM7938, bandwidth: 40 GHz). The output signal from the MZM is sent to a PD (CONQUER Inc., bandwidth: 10 GHz) to implement photonic frequency mixing. The dechirped signal is filtered by an LPF having a bandwidth of 100 MHz. Then, the dechirped signals are sampled by a four-channel real-time oscilloscope (Agilent, DS09404) with a sampling rate of 500 MSa/s in each channel.

First of all, a metallic plane with a size of 6 cm × 7 cm is used as the target, which is placed at a distance of about 2.1 m from the ULA ($\theta_s = 0°$). According to Eqs. (7) and (8), the theoretical resolution of the image is 3.75 cm in range direction and 2.57° in azimuth direction. In the experiment, the target has a size much smaller than that determined by the distance and the azimuth resolution. Thus, it can be treated as a point target to perform the digital TTD compensation. Figures 4(a)-4(d) show the sampled waveforms of the four dechirped signals in a temporal period of 10 μs, based on which four 1D range profiles are calculated according to Eq. (1). Here the low-frequency envelope in Fig. 4(d) is generated due to the imperfect performance of the PD in the fourth receive channel. While, this does not affect the radar performance since its frequency is much lower than the frequency of the de-chirped signal. After digital true time delay compensation, the obtained four 1D range profiles

Optics EXPRESS

are shown in Figs. 4(e)-4(h). As can be seen, in each curve, a peak corresponding to the target is observed at the distance of 2.099 m.

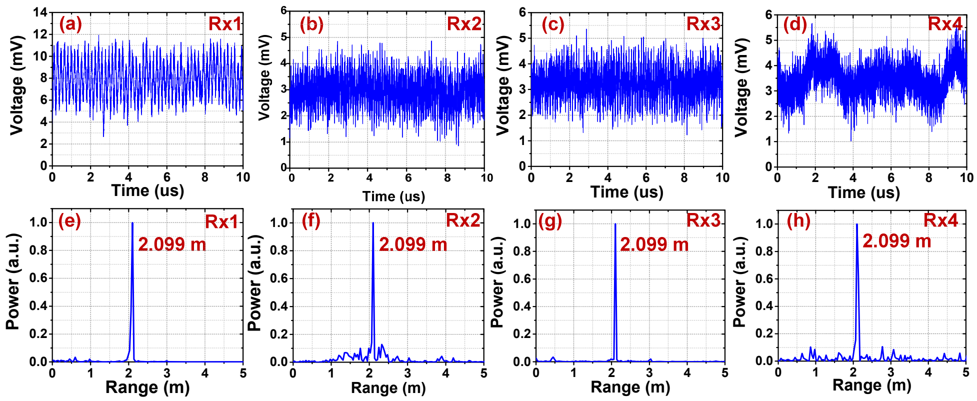

Fig. 4. The sampled waveform of (a) Rx1, (b) Rx2, (c) Rx3 and (d) Rx4; and the 1D range profiles after digital TTD compensation of (e) Rx1, (f) Rx2, (g) Rx3 and (h) Rx4.

Based on Eqs. (4)-(6), a 2D image is constructed by sweeping with a step of 3.75 cm (the theoretical range resolution) in the range direction and a step of 0.01° in the azimuth direction. The obtained image with a total viewing angle of 32° is shown in Fig. 5(a). Obviously, three bright spots appear at a distance of 2.099 m. The central spot is the target image formed by the main lobe of the beam, while the other two are duplications due to the ± 1st-order grating lobes. In this experiment, because of the large volume of the horn antennas, the element spacing (d) of the ULA is 6.2 cm, which is about 4.96 times of the central wavelength. Thus, grating lobes are inevitable in the obtained image. According to the theory in [22], the angles of the ± 1st grating lobes are estimated to be ± 11.631°, which are consistent with the result in Fig. 5. In practical applications, the grating lobe images can be eliminated by applying small-size antennas to get a small value of d or applying the unequally spaced phased array technique [23,24]. In Fig. 5(a), the areas with weak brightness are due to the sidelobes, which is determined by the rectangular envelops of the sampled singles shown in Fig. 4. Then, the point spread function (PSF) [25] of the established phased array radar is analyzed through the central spot area in Fig. 5(a). Figures 5(b) and 5(c) show the profiles of the PSF along the range direction and the azimuth direction, respectively. Through the full width at half maximum (FWHM) of the two curves, the range resolution and azimuth resolution are estimated to be 3.85 cm and 2.68°, respectively, which are very close to the theoretical values. It should be noted that, the sidelobes in azimuth profile in Fig. 5(c) has a strong amplitude, because they are actually the superimposition of the lobes beside the main and grating lobes. In practical applications, by eliminating the grating lobes or separating the grating lobes from the main lobe, amplitude of the sidelobes can be reduced.

Optics EXPRESS

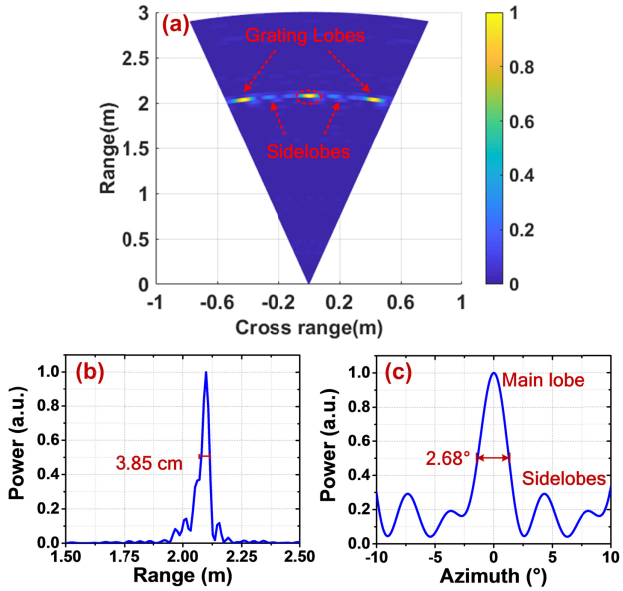

Fig. 5. (a) Imaging result of the single metallic plane, (b) profiles of the PSF along the range direction, (c) profiles of the PSF along the azimuth direction.

Based on the established photonics-based phased array radar, imaging of multiple targets is also demonstrated. In the experiment, four metallic planes with a size of 6 cm × 7 cm are used as the targets. The photographs in Figs. 6(a)-7(c) show the four metallic planes placed at different positions. The constructed images are also shown in Fig. 6. In the image results of Fig. 6, the grating lobes are not shown by setting the viewing angle to be ~13.6°. As can be seen, despite of the existence of sidelobes in these images, the position of each metallic plane can be well recognized, and the patterns composed by the four metallic planes are clearly displayed.

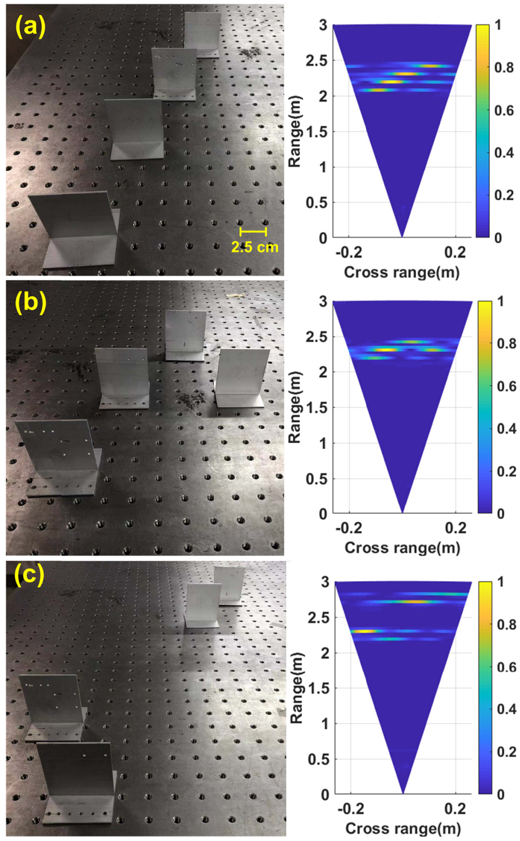

Fig. 6. (a), (b) and (c) Photographs of the four metallic planes placed in different positions, and the corresponding imaging results.

4. Discussion and conclusion

For the proposed phased array radar, the range resolution can be improved by choosing a large operation bandwidth. Due to hardware constraints, a 4-GHz bandwidth phased array radar is demonstrated in the experiment, which leads to a range resolution of 3.85 cm. While, the LFM signal generation and processing in this system can achieve a much larger bandwidth, e.g., a photonics-based Ka-band radar with a bandwidth of 12 GHz has been demonstrated to achieve a range resolution as high as 1.3 cm [26]. As for azimuth resolution, it is determined by the number of receive elements once the element spacing is fixed. To show this property, a two-target (two metallic planes) imaging experiment is implemented. Figure 7(a) shows the image obtained by the four-element receive array as previously demonstrated, while Fig. 7(b) shows the image obtained by a two-element receive array having the same element spacing. Comparing the results in Fig. 7, it is obvious that the image obtained by the four-element receive array has a much higher azimuth resolution. Specifically, the azimuth resolution is decreased from 2.68° to 5.87°, when the element number changes from 4 to 2. Therefore, the azimuth resolution can be improved by applying more receive elements to form a larger equivalent radar aperture, e.g., a 102-element phased array can achieve an azimuth resolution of 0.1°.

Optics EXPRESS

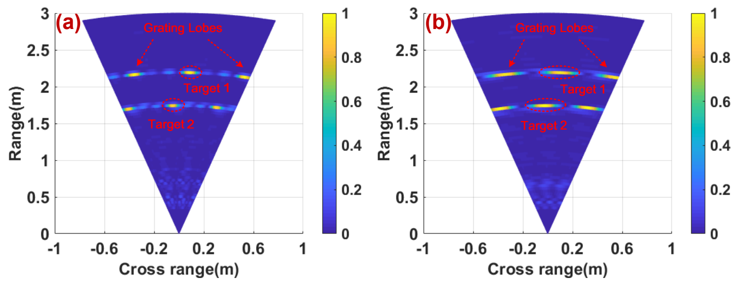

Fig. 7. Imaging results by (a) a 4-element phased array radar, (b) a 2-element phased array radar.

In conclusion, we have demonstrated a photonics-based phased array radar for high-resolution imaging based on broadband digital beamforming. In the experiment, a photonics-based 1 × 4 phased array radar with a bandwidth of 4 GHz (22-26 GHz) was established. The range and azimuth resolution of the phased array radar were evaluated, and imaging of multiple targets are also demonstrated. The results can verify the feasibility of the proposed system, which is a promising solution to implementing broadband beam steering and imaging in a phased array radar.

Funding

National Natural Science Foundation of China (61871214); Natural Science Foundation of Jiangsu Province (BK20180066); Jiangsu Provincial Program for High-level Talents in Six Areas (DZXX-005); Jiangsu Provincial "333" Project (BRA2018042); Fundamental Research Funds for the Central Universities (NS2018028).

References

1. S. Stanko, D. Notel, A. Wahlen, J. Huck, F. Kloppel, R. Sommer, and M. Hagelen, "Active and passive mm-wave imaging for concealed weapon detection and surveillance," in 2008 33rd International Conference (IEEE IRMMW-THz, 2008).
2. J. Dickmann, N. Appenrodt, H. Bloecher, C. Brenk, T. Hackbarth, M. Hahn, J. Klappstein, M. Muntzinger, and A. Sailer, "Radar contribution to highly automated driving," in 2014 44th European Microwave Conference (EuMC, 2014).
3. P. Ghelfi, F. Laghezza, F. Scotti, G. Serafino, S. Pinna, D. Onori, E. Lazzeri, and A. Bogoni, "Photonics in radar systems," IEEE Microw. Mag. **16**(8), 74–83 (2015).
4. L. Zhuang, C. G. Roeloffzen, A. Meijerink, M. Burla, D. A. Marpaung, A. Leinse, M. Hoekman, R. G. Heideman, and W. van Etten, "Novel ring resonator-based integrated photonic beamformer for broadband phased array receive antennas—Part II: Experimental prototype," J. Lightwave Technol. **28**(1), 19–31 (2010).
5. C. Jose and N. Dovak, "Microwave photonics combines two worlds," Nat. Photonics **1**(6), 319–330 (2007).
6. J. Yao, "Microwave photonics," J. Lightwave Technol. **27**(3), 314–335 (2009).
7. P. Ghelfi, F. Laghezza, F. Scotti, G. Serafino, A. Capria, S. Pinna, D. Onori, C. Porzi, M. Scaffardi, A. Malacarne, V. Vercesi, E. Lazzeri, F. Berizzi, and A. Bogoni, "A fully photonics-based coherent radar system," Nature **507**(7492), 341–345 (2014).
8. F. Zhang, Q. Guo, and S. Pan, "Photonics-based real-time ultra-high-range-resolution radar with broadband signal generation and processing," Sci. Rep. **7**(1), 13848 (2017).
9. W. Zou, H. Zhang, X. Long, S. Zhang, Y. Cui, and J. Chen, "All-optical central-frequency-programmable and bandwidth-tailorable radar," Sci. Rep. **6**(1), 19786 (2016).
10. X. Ye, F. Zhang, Y. Yang, and S. Pan, "Photonics-based radar with balanced I/Q de-chirping for interference-suppressed high-resolution detection and imaging," Photon. Res. **7**(3), 265–272 (2019).
11. F. Zhang, Q. Guo, Z. Wang, P. Zhou, G. Zhang, J. Sun, and S. Pan, "Photonics-based broadband radar for high-resolution and real-time inverse synthetic aperture imaging," Opt. Express **25**(14), 16274–16281 (2017).
12. F. Zhang, Q. Guo, Y. Zhang, Y. Yao, P. Zhou, D. Zhu, and S. Pan, "Photonics-based real-time and high resolution ISAR imaging of non-cooperative target," Chin. Opt. Lett. **15**(11), 112801 (2017).
13. X. Xiao, S. Li, B. Chen, X. Yang, D. Wu, X. Xue, X. Zheng, and B. Zhou, "A microwave photonics- based inverse synthetic aperture radar system," in 2017 CLEO: Science and Innovations, paper. JW2A.144.
14. F. Zhang, B. Gao, and S. Pan, "Photonics-based MIMO radar with high-resolution and fast detection capability," Opt. Express **26**(13), 17529–17540 (2018).

Optics EXPRESS

15. X. Xiao, S. Li, S. Peng, D. Wu, X. Xue, X. Zheng, and B. Zhou, "Photonics-based wideband distributed coherent aperture radar system," Opt. Express **26**(26), 33783–33796 (2018).
16. Z. Tegegne, C. Bin, T. Fromenteze, and C. Berthelemot, "Single Channel Microwave Photonics Digital Beamforming Radar Imaging System," J. Lightwave Technol. **36**(3), 675–681 (2018).
17. X. Ye, F. Zhang, and S. Pan, "Optical true time delay unit for multi-beamforming," Opt. Express **23**(8), 10002–10008 (2015).
18. X. Ye, F. Zhang, and S. Pan, "Compact optical true time delay beamformer for a 2D phased array antenna using tunable dispersive elements," Opt. Lett. **41**(17), 3956–3959 (2016).
19. P. Maak, I. Frigyes, L. Jakab, I. Habermayer, M. Gyukics, and P. Richter, "Realization of true-time delay linesbased on acoustooptics," J. Lightwave Technol. **20**(4), 730–739 (2002).
20. S. Chin, L. Thévenaz, J. Sancho, S. Sales, J. Capmany, P. Berger, J. Bourderionnet, and D. Dolfi, "Broadband true time delay for microwave signal processing, using slow light based on stimulated Brillouin scattering in optical fibers," Opt. Express **18**(21), 22599–22613 (2010).
21. Q. Guo, F. Zhang, P. Zhou, and S. Pan, "Dual-band LFM signal generation by frequency quadrupling and polarization multiplexing," IEEE Photonics Technol. Lett. **29**(16), 1320–1323 (2017).
22. C. Balanis, Antenna Theory: Analysis and Design (John Wiley & Sons Inc., 2016).
23. F. Zhang, D. Zhang, and S. Pan, "Fast and wide-range optical beam steering with ultralow side lobes by applying an optimized multi-circular optical phased array," Appl. Opt. **57**(18), 4977–4984 (2018).
24. S. Yin, J. Kim, F. Wu, P. Ruffin, and C. Luo, "Ultra-fast speed, low grating lobe optical beam steering using unequally spaced phased array technique," Opt. Commun. **270**(1), 41–46 (2007).
25. R. Racine, "The telescope point spread function," Publ. Astron. Soc. Pac. **108**(726), 699–705 (1996).
26. Y. Yao, F. Zhang, Y. Zhang, X. Ye, D. Zhu, and S. Pan, "Demonstration of ultra-high-resolution photonics-based Ka-band inverse synthetic aperture radar imaging," in 2018 Optical Fiber Communication Conference (OFC2018), paper. Th3G.5.